Geol. Mag. **140** (*1*), *2003, pp. 11–24.* © *2003 Cambridge University Press*
DOI: 10.1017/S0016756802006994 *Printed in the United Kingdom*

Geochemistry of a Tertiary continental basalt suite, Red Sea coastal plain, Egypt: petrogenesis and characteristics of the mantle source region

ABDEL-KADER M. MOGHAZI*

Department of Geology, Faculty of Science, Alexandria University, Alexandria, Egypt

(*Received* 11 September 2001; *accepted* 2 September 2002)

Abstract – Major and trace element data on Tertiary continental basalt flows from the Shalatein area, Red Sea coastal plain of Egypt, have been presented and used to obtain more information about their source region and the processes involved in their generation. The rocks are mainly alkali olivine basalt with MgO and Mg no. in the range of 9.8–5 wt% and 65–46, respectively. They display wide variations in incompatible element concentrations, particularly LREE, Zr, Nb, K, Y, Ba and Sr. There is no evidence of significant crustal contamination or a lithospheric mantle signature in these rocks. Normalized trace element patterns and diagnostic elemental ratios are very similar to those of modern ocean-island basalts (OIB) a feature which suggests that the mantle source region was the asthenosphere. Comparison with the different types of OIB indicates that the basalts may be derived from a high U/Pb (HIMU) source with slightly elevated K and Ba contents. The basalts show general trends of increasing incompatible elements (K_2O, Nb, Y, Sr and Yb), and decreasing contents of compatible elements (Cr, Ni, Sc and Ca) with decreasing Mg no. Furthermore, TiO_2, P_2O_5, LREE and Th define maxima at about Mg no. = 56, suggesting late fractionation of Fe–Ti oxides and apatite. Although these variations are consistent with fractional crystallization processes, the wide variations in LREE contents and the incompatible trace element ratios Ce/Y (1.2–3.8), Zr/Nb (2.3–7.1) and Nb/Y (0.6–4) in the least fractionated samples (Mg no. > 56) suggest that fractional crystallization involving the observed phenocryst assemblage (olivine and clinopyroxene) cannot fully explain such compositional variations. Modelling of the mafic rocks (Mg no. > 56) using REE suggests varying degrees of partial melting of an enriched mantle source region in the garnet stability field. Partial melting is attributed to plume-related mantle upwelling beneath the Red Sea rift system.

Keywords: geochemistry, Tertiary, basalts, Red Sea, rift valleys, Egypt.

1. Introduction

Continental basalts are commonly associated with tectonically active areas that ultimately undergo rifting (Gieret & Lameyre, 1985). These basalts can provide an integrated record of the different processes involved in the evolution of the continental lithosphere. Most preserved continental basalt provinces are of Mesozoic and Tertiary age and seem to be related in some way to breakup of continents (MacDougall, 1988). The presence of Mesozoic continental basalts in the Red Sea area has been documented in several places (Almond, 1986; Franz, Puchelt & Pasteels, 1987; Hubbard, Wood & Rogers, 1987; Moghazi, Hassanen & Mohamed, 1997; Mohamed, 2001). However, the Tertiary was a time of intense tectonic and magmatic activity in the region. The main tectonic effects are initiation of many extension-related faults, reactivation of the pre-existing NW-, NE- and E–W-trending faults and opening of the Red Sea basin via rifting of the Arabian–Nubian Shield (Bohannon, 1986; Camp & Robool, 1991). Voluminous magmatism, contemporaneous with the opening of the Red Sea, began about 30 Ma and was manifested by several basaltic lava fields and dyke swarms on both sides of the Red Sea (Coleman *et al*. 1977; Pallister, 1987). These lava fields dominate the western part of the Arabian Peninsula, and comprise one of the largest continental basalt provinces in the world (Coleman, Gregory & Brown, 1983). Additional geological mapping and geochronological studies in Egypt conducted by many investigators (e.g. Meneisy & Kreuzer, 1974; Franz, Puchelt & Pasteels, 1987; Meneisy, 1990; Baldridge *et al*. 1991) resulted in the recognition of a widespread group of Tertiary basalts (that is, 30–15 Ma). These Tertiary basalts, mainly related to the Red Sea rifting, extend from the extreme northern part in Sinai to the extreme southern part of Egypt (Fig. 1). There is no correlation between the age of the basalts and their geographic distribution.

Over the last ten years there has been increasing interest in studies of the Tertiary basaltic rocks around the Red Sea–Gulf of Aden (e.g. Camp & Robool, 1991; Baker, Snee & Menzies, 1996; Volker *et al*. 1997; Ghebreab, 1998; Haase, Muhe & Stoffers, 2000). Most

*E-mail: moghazi_16@yahoo.com

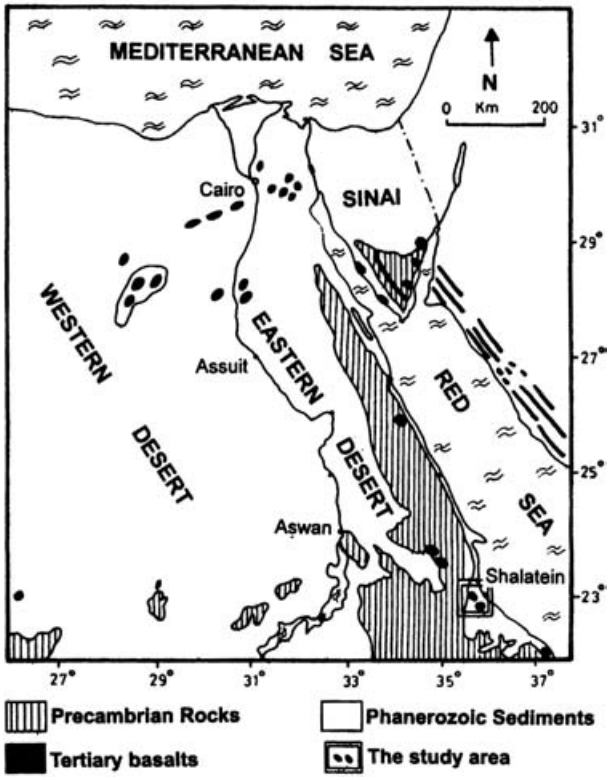

Figure 1. Map showing the location of the study area in relation to the main Tertiary volcanic occurrences in Egypt and western Saudi Arabia.

of these studies have been carried out in an attempt to understand the tectonic and magmatic processes that accompanied continental rifting and the transition from continental to oceanic magmatism. This paper is a further consideration of basalts from the Red Sea region. It examines, in particular, the geology, petrography and geochemistry of an alkali olivine basalt suite from the Shalatein area along the Red Sea coastal plain in southern Egypt. The aim is to place constraints on the geochemical evolution of these basaltic magmas. The field and petrographic data combined with the geochemical results allow speculation on the tectonic significance of this basalt suite.

2. Geological setting

2.a. General

Tertiary magmatism in Egypt is uniformly basaltic in composition and widely distributed north of latitude 28° N (Fig. 1). The basaltic rocks occur mainly in the form of lava flows, dykes, sills, small irregular stocks, plugs and cinder cones. They occur sporadically over a large area beneath the Nile delta and the adjacent parts of the Western Desert (Meneisy, 1990). In the extreme southern parts of the Western Desert, some of these basaltic occurrences are sparsely distributed (Franz, Puchelt & Pasteels, 1987). In Sinai, Tertiary basalts occur in the southern and southeastern parts as dykes, few sills, plugs and small flow remnants covering Precambrian rocks and Phanerozoic sediments (Baldridge *et al*. 1991). Along the Red Sea coast, some basaltic flows, dykes and plugs occur to the south of Quseir and at Shalatein (Ressetar, Narin & Monard, 1981; Abdel Aal, 1988). Three Tertiary volcanic episodes in Egypt may be distiguished from K–Ar age data compiled by Meneisy (1990): (1) Late Eocene–Early Oligocene phase (40 ± 10 Ma), (2) Oligo-Miocene phase (24 ± 2 Ma) and (3) Lower–Middle Miocene phase (20–15 Ma). Based on the results of several geochemical studies of the Tertiary basalts in Egypt (e.g. El Hinnawi & Abdel Maksoud, 1972 Abdel Monem & Heikal, 1981; Franz, Puchelt & Pasteels, 1987; Hafez & Abdou, 1990; Baldridge *et al*. 1991; Hanafy, Yousef & Gad, 1996), two within-plate continental magma types are distinguished, namely, alkali olivine basalt and tholeiitic magmas.

Details of the geology of the Red Sea coastal plain in Egypt are presented in a number of studies (e.g. Said, 1962, 1990; Purser, Philobbos & Soliman, 1990; Purser & Philobbos, 1993; Ouda & Masoud, 1993). These studies are concerned only with the record of Red Sea rifting preserved in sedimentary rocks of mostly Tertiary age. The general stratigraphy of the Egyptian Red Sea coastal plain is shown in Figure 2. As shown in this stratigraphic column, basalt flows are intercalated with sediments in the Oligo-Miocene Abu Ghusun Formation.

2.b. The study area

The study area lies close to Shalatein town, along the Red Sea coastal plain, southern Egypt (Fig. 1). The main geomorphological features of the area include: (1) the Wadi Hodein alluvial fan, which lies over a large area (100 km^2), and is mainly composed of Recent sediments and weathering materials from the basement rocks; (2) the Red Sea coastal plain, which includes reefs, sabkha and sand sheets; and (3) dissected hills (20–30 m high) of basement rocks, sedimentary rocks and basalt flows. The dissected hills are classified (Abu Zeid *et al*. 2000) into the following stratigraphic units (Fig. 3), from the older to the younger: (1) Basement rocks (Late Precambrian), mainly represented by metavolcanic rocks and granites; (2) Nubia Formation (Cretaceous), mainly sandstone and grit; (3) Abu Ghusun Formation (Oligo-Miocene), mainly clastic sediments covered by basalt flows; (4) Old Reefs (Pleistocene); and (5) Alluvium deposits and Sabkha (Holocene).

The Abu Ghusun Formation generally consists of siliciclastic sediments (including fluviatile grits, conglomerates, ferruginous sandstone and siltstone) overlain by basalts (Purser & Philobbos, 1993). This formation is considered to be composed of proto-rift sediments (Orszag & Plaziat, 1990). The following section of the Abu Ghusun Formation was measured at the

https://doi.org/10.1017/S0016756802006994 Published online by Cambridge University Press

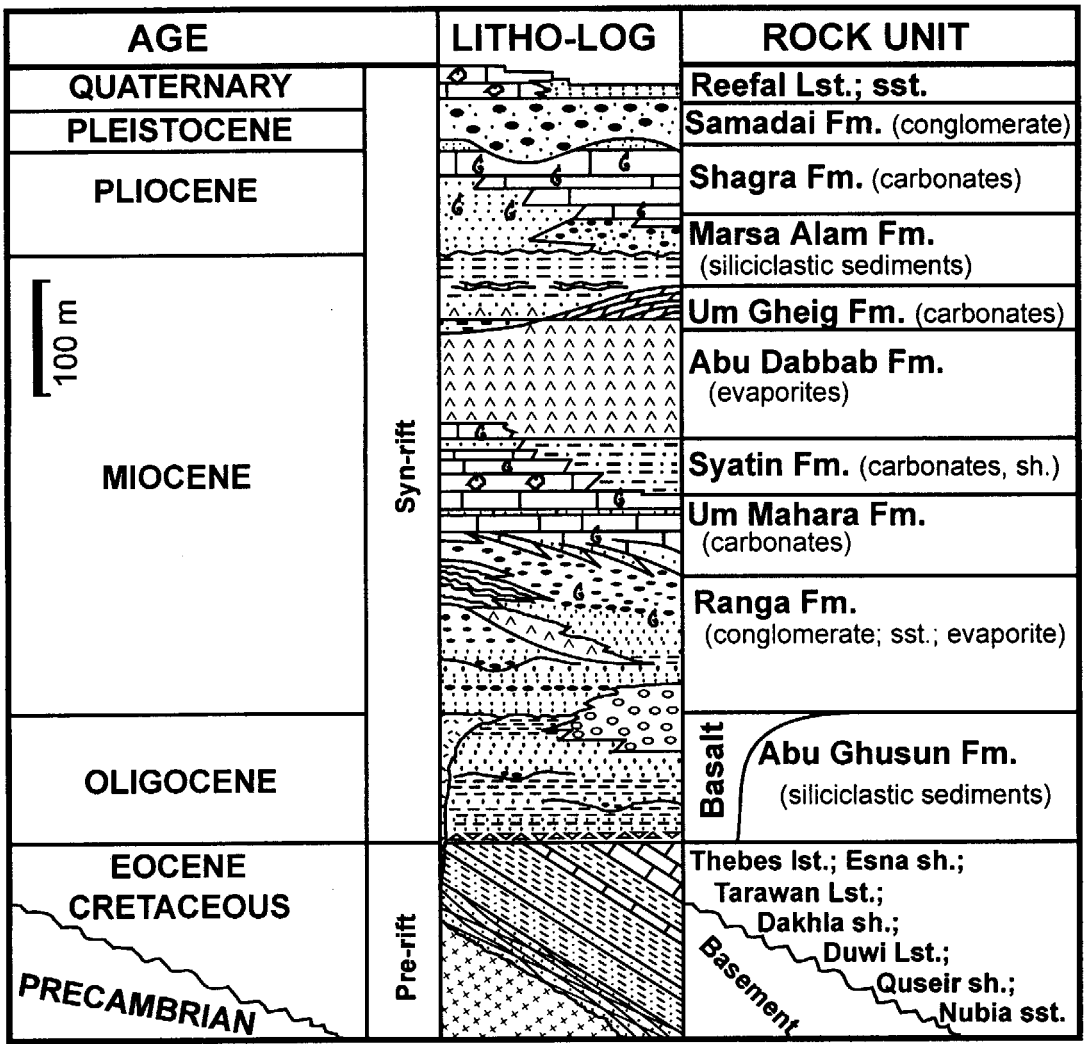

Figure 2. Stratigraphy of the Egyptian Red Sea coastal region (modified from Purser & Philobbos, 1993).

Shalatein area, starting from the base: (1) red to white conglomerates (6–8 m thick); (2) highly fractured and weathered basalt flows (15–20 m thick), in the form of disconnected outcrops. Texturally, the basalts are massive and porphyritic; vesicular textures are occasionally observed.

The structural pattern of the area is mainly governed by faulting. The regional fault pattern trends are predominantly 320° and 60°. These faults are of the normal type and juxtapose Phanerozoic sediments of different ages against each other, and against Precambrian basement rocks. The basalt outcrops are mostly arranged parallel to the 320° fault pattern (Fig. 3).

3. Petrography

The basalts in the different exposures are mineralogically similar and consist almost entirely of olivine basalts. They are generally porphyritic to subaphyric; aphyric rocks are very scarce. The groundmass consists of plagioclase laths, clinopyroxene, olivine, Fe–Ti oxides and occasional interstitial glass. Most of the samples show a slight to a very pronounced sub-parallel orientation of the plagioclase laths. Vesicular and/or amygdaloidal textures are occasionally recorded. Zeolites (natrolite) and carbonate minerals (calcite) occur in some samples in the groundmass as well as in amygdales. The phenocrysts are olivine, clinopyroxene, Fe–Ti oxides and occasionally plagioclase. There is no obvious horizontal variation in the composition of the basalts; however, within-flow vertical variation, represented by change in phenocryst types and proportions, is recorded. Basalts with only olivine phenocrysts occur at the base, followed by basalt with olivine, clinopyroxene, magnetite and plagioclase phenocrysts.

Olivine phenocrysts (1–5 mm long), in the form of euhedral to subhedral-elongated crystals, occur in all samples. They are the dominant phenocryst phase in the most mafic samples and occur together with clinopyroxene and plagioclase in the more evolved rocks. The olivine phenocrysts are mostly fresh and may contain dark green spinel inclusions. In some samples, partial alteration of olivine, along cracks and crystal margins, to a brown pseudomorph (iddingsite) and

https://doi.org/10.1017/S0016756802006994 Published online by Cambridge University Press

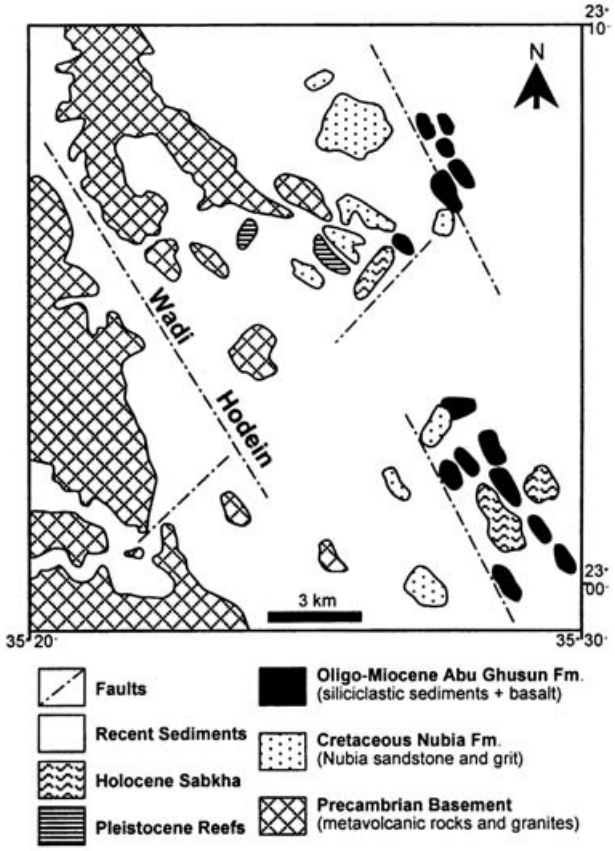

Figure 3. Geological map of the study area (modified from Abu Zeid *et al*. 2000).

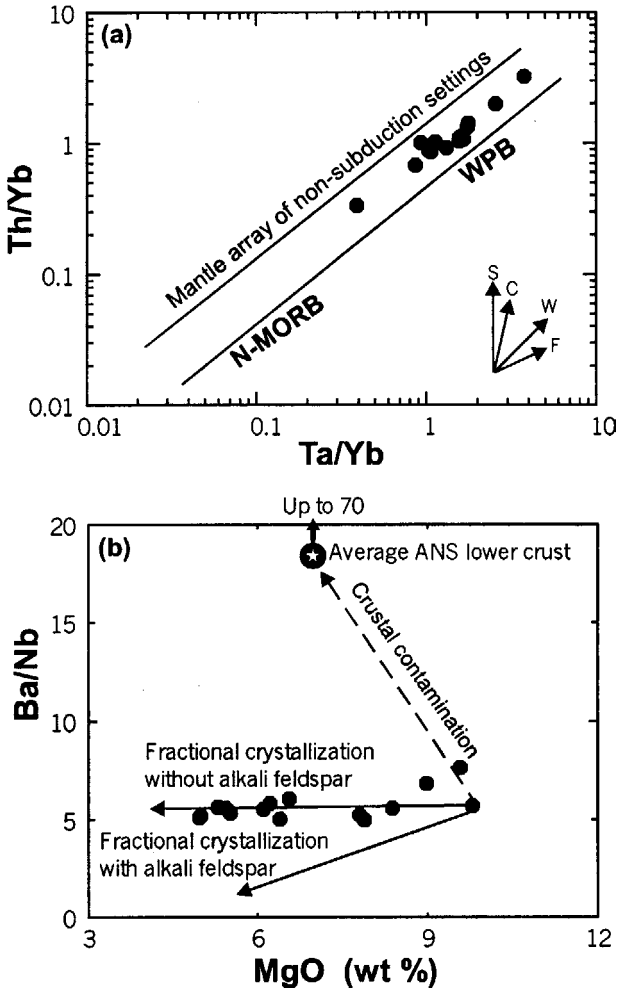

Figure 4. (a) Ta/Yb v. Th/Yb diagram after Pearce (1983); vectors show trends produced by subduction zone enrichment (S), crustal contamination (C), within-plate enrichment (W) and fractional crystallization (F). WPB – within-plate basalts. (b) MgO (wt%) v. Ba/Nb; solid line vectors show the expected trends for fractional crystallization, whereas the dashed line vector shows the expected trend of crustal contamination. Average Arabian–Nubian Shield (ANS) lower crust is from McGuire & Stern (1993).

serpentine-chlorite is common. Clinopyroxene phenocrysts (1–8 mm long), exhibiting ophitic to subophitic textures, are pink and euhedral to subhedral. They are twinned and/or zoned short prismatic crystals that often form groups or clusters, accompanied by oxide inclusions.

Oxides are present in all the rocks. In the most mafic samples, the oxide phase is represented by small inclusions of spinel in olivine. More evolved rocks contain magnetite (up to 3 mm long) and titanomagnetite (1 mm long), both as inclusions in clinopyroxene phenocrysts or as interstitial grains. Exsolved ilmenite lamellae are common in the titanomagnetite. Some olivine–clinopyroxene–phyric samples contain abundant ilmenite. Plagioclase (up to 1 cm long) is a dominant phenocryst phase in the more evolved rocks. Like other phenocryst phases, plagioclase occurs as euhedral to subhedral prismatic to tabular crystals. In contrast to the unzoned plagioclase laths in the groundmass, the plagioclase phenocrysts are usually twinned and zoned. Apatite in the form of short prisms and minute six-sided crystals is frequently observed as inclusions in clinopyroxene phenocrysts.

4. Geochemistry

Based on the petrographic investigations, 15 representative samples covering the different basalt varieties were selected for major and trace element analyses. Major element compositions and Sc, Ba and Ni abundances were determined by inductively coupled plasma-atomic emission spectrometry (ICP-AES). The remainder of trace elements and the rare earth elements (REE) were determined by inductively coupled plasma-mass spectrometry (ICP-MS). All the analyses were carried out at the ACME Analytical Laboratories Ltd, Canada. Analytical precision, as calculated from replicate analyses, is 0.5% for major elements and varies from 2–5% for trace elements of > 80 ppm, 2–10% for trace elements of 10–80 ppm and 5–20% for trace elements of <10 ppm. The analytical data, CIPW norms and laboratory values for the the Shalatein basalt samples, as well as values for the international rock standard SO-15/CBS, are given in Tables 1 and 2.

https://doi.org/10.1017/S0016756802006994 Published online by Cambridge University Press

Table 1. Chemical data of major oxides, CIPW norms and trace elements for the Shalatein Tertiary basalts

Sample	SH-14	SH-15	SH-8	SH-16	SH-1	SH-2	SH-10	SH-5	SH-3	SH-17	SH-7	SH-9	SH-11	SH-12	SH-13	SO-15*
SiO_2	44.80	45.80	44.66	46.88	46.33	44.09	47.68	46.44	45.52	46.50	46.35	46.11	46.51	47.07	47.00	49.55
TiO_2	1.69	1.43	2.65	2.01	2.54	3.30	2.23	2.48	2.70	1.99	2.65	1.94	2.00	2.55	2.60	1.71
Al_2O_3	14.86	15.29	14.83	15.33	15.09	13.12	16.22	16.66	16.58	18.29	16.55	18.31	18.38	17.08	17.13	12.46
Fe_2O_3	10.27	10.71	11.44	10.75	11.16	12.14	10.86	10.80	11.73	10.24	11.71	9.95	10.21	11.33	11.68	7.31
MnO	0.15	0.16	0.16	0.16	0.16	0.18	0.16	0.16	0.17	0.15	0.17	0.14	0.15	0.17	0.18	1.39
MgO	9.79	9.50	8.98	8.38	7.80	7.88	6.56	6.22	6.39	5.52	6.10	5.30	5.44	4.97	4.99	7.16
CaO	10.72	10.11	9.69	8.39	8.28	11.35	8.19	9.61	9.32	11.67	8.61	11.24	10.96	8.38	8.39	5.82
Na_2O	2.69	2.85	3.17	3.25	4.09	4.37	3.88	2.97	3.61	3.09	3.39	3.15	3.01	3.44	3.36	2.38
K_2O	0.66	0.53	1.04	1.09	1.50	1.24	1.11	0.85	1.12	1.11	1.18	1.02	1.04	1.33	1.24	1.97
P_2O_5	0.21	0.16	0.41	0.46	0.50	0.78	0.45	0.32	0.41	0.25	0.44	0.26	0.25	0.44	0.45	2.68
Mg no.	65	64	61	61	58	56	54	53	52	52	51	51	51	46	46	
Na_2O/K_2O	4.1	5.4	3.0	3.0	2.7	3.5	3.5	3.5	3.2	2.8	2.9	3.1	2.9	2.6	2.7	
Na_2O+K_2O	3.4	3.4	4.2	4.3	5.6	5.6	5.0	3.8	4.7	4.2	4.6	4.2	4.0	4.8	4.6	
or	3.9	3.1	6.2	6.4	8.3	7.3	6.6	5.0	6.6	6.6	7.0	6.0	6.2	7.9	7.3	
ab	18.8	22.7	21.0	27.5	25.3	13.9	32.8	25.1	25.1	20.1	28.7	22.0	23.5	29.1	28.4	
an	26.5	27.4	23.2	24.0	18.4	12.5	23.6	29.6	25.7	32.8	26.5	32.8	33.6	27.2	28.0	
ne	2.1	0.8	3.2	–	5.1	12.2	–	–	3.0	3.3	–	2.5	1.1	–	–	
di	20.2	17.5	17.6	11.7	15.5	30.6	11.3	12.7	14.3	18.9	10.7	17.0	15.4	9.2	8.6	
hy	–	–	–	3.8	–	–	0.1	8.3	–	–	2.4	–	–	6.1	8.1	
ol	15.3	17.0	13.2	12.6	11.9	5.9	11.6	3.8	10.0	7.2	9.1	6.8	8.2	4.8	3.9	
mt	4.6	4.3	6.0	5.1	5.9	7.0	5.4	5.8	6.1	5.1	6.0	5.0	5.1	5.9	5.9	
il	3.2	2.7	5.0	3.8	4.8	6.3	4.2	4.7	5.1	3.8	5.0	3.7	3.8	4.8	4.9	
ap	0.5	0.4	1.0	1.1	1.2	1.8	1.1	0.7	1.0	0.6	1.0	0.6	0.6	1.0	1.1	
Cr	229	164	192	161	157	120	92	62	72	65	72	62	62	34	34	3633
Ni	211	221	239	233	186	123	128	68	112	76	89	68	83	52	44	79
Co	51	52	53	44	45	49	40	41	44	41	40	37	41	39	36	22
Sc	31	29	23	19	17	22	20	22	20	24	17	23	24	15	15	12
V	225	220	224	157	200	254	155	226	230	223	201	209	216	192	187	144
Rb	9	5	18	19	26	20	16	16	20	15	20	13	15	22	21	65
Cs	0.1	0.2	0.3	0.2	0.5	0.6	0.3	0.2	0.2	0.2	0.4	0.3	0.2	0.6	0.6	2.8
Ba	114	94	335	218	335	499	218	239	277	155	310	158	162	312	312	2007
Sr	428	391	665	708	665	847	658	595	806	607	810	617	603	918	988	409
Ga	16	16	21	19	22	20	17	22	20	21	20	21	20	22	20	17
Ta	1.4	0.7	3.3	3.4	4.5	6.5	2.4	3.0	3.6	2.1	3.7	1.9	2.1	4.2	4.0	1.9
Nb	20	11	49	39	64	100	36	41	55	29	56	28	29	61	60	33
Hf	2.4	1.8	4.6	5.4	5.5	5.8	4.8	4.8	4.5	3.2	5.2	3.2	3.7	5.6	4.9	26.4
Zr	94	78	172	222	237	231	186	171	180	132	193	125	129	209	209	1062
Y	18	18	21	22	21	25	25	23	23	19	25	19	19	27	27	22
Th	1.1	0.6	2.5	2.2	3.5	5.6	2.6	2.1	2.9	1.7	2.6	1.6	1.9	2.8	2.8	23.5
U	0.7	0.1	0.8	0.8	1.1	1.9	0.7	0.5	0.8	0.5	0.9	0.5	0.6	0.9	0.9	20.9

Fe_2O_3 is the total iron as Fe_2O_3; * International rock standard.

4.a. Alteration and crustal contamination

Alteration and crustal contamination are secondary processes, which may have contributed to the chemical composition of the Shalatein basalt suite. These processes should be considered before reliable information about the source region and evolution processes can be extracted from the rock analyses.

Unaltered olivine was visible in all samples selected for chemical analysis, and alteration is considered negligible. It is important also to assess whether or not the basalts have undergone crustal contamination. This is because most of the rock varieties are porphyritic, suggesting that they might have resided in crustal magma chambers prior to eruption and would thus have had adequate opportunity to interact with continental crust via assimilation–fractional crystallization (AFC) processes. For this purpose, evidence from incompatible trace elements such as Th, Ta and Yb will be considered. Crustal contamination affects Th more than Ta and Yb, leading to displacement towards high Th/Yb values. Figure 4a shows the variation of Th/Yb v. Ta/Yb (Pearce, 1983). MORB and uncontaminated intra-plate basalts plot in a well-defined array, indicating that mantle enrichment events appear to equally concentrate Ta and Th (Wilson, 1989). In contrast, contaminated basalts will be displaced towards higher Th/Yb values due to the influence of crustal materials enriched in Th. All the analysed samples plot inside the mantle array field (Fig. 4a) suggesting negligible crustal contamination.

The large ion lithophile elements (LILE) such as Rb, Ba and K and the high field strength elements (HFSE) such as Zr and Nb are incompatible with respect to the phenocryst phases in the investigated basalts. Davidson *et al*. (1987, 1988) argue that ratios like Ba/Nb and Rb/Zr will not significantly change by simple fractional crystallization in basaltic rocks, while variations in these ratios will be related to crustal contamination by AFC processes. Figure 4b shows that most of the samples have no significant variation in Ba/Nb ratios with decreasing MgO. Also, assimilation of crustal rocks should produce an increase in the Ba/Nb ratios with decreasing MgO along the line labelled ‘crustal contamination’ in Figure 4b. The absence of such a trend implies that crustal contamination did not play a major role in the evolution of the Shalatein basalts.

https://doi.org/10.1017/S0016756802006994 Published online by Cambridge University Press

Table 2. Concentrations of rare earth elements in the Shalatein Tertiary basalts

Sample	SH-14	SH-15	SH-7-1	SH-16	SH-1	SH-2	SH-10	SH-5	SH-3	SH-17	SH-7	SH-9	SH-11	SH-12	SH-13	SO-15*
La	10.30	6.90	24.10	22.30	30.10	49.10	24.50	20.00	26.40	15.20	24.20	15.20	16.00	24.90	25.00	28.00
Ce	22.30	15.60	50.00	47.70	59.90	95.80	51.30	41.80	55.10	33.00	49.90	32.80	33.00	53.20	51.60	58.40
Pr	2.85	2.12	5.69	5.52	7.07	10.77	6.03	5.09	6.44	4.05	5.98	3.96	3.91	6.29	6.03	6.05
Nd	12.50	10.40	24.10	23.20	29.00	42.20	25.10	22.00	26.80	17.30	24.90	17.20	16.60	26.40	25.20	22.50
Sm	3.00	2.60	5.10	4.40	6.30	7.40	5.20	4.90	4.50	3.80	5.20	3.60	3.70	5.40	5.60	4.20
Eu	1.33	1.05	1.99	1.85	2.09	3.00	2.06	1.89	2.09	1.53	2.05	1.66	1.69	2.16	1.97	0.98
Gd	3.21	2.99	5.13	4.78	5.42	7.22	5.36	4.99	5.26	3.91	5.18	3.91	4.16	5.39	5.19	3.93
Tb	0.52	0.50	0.78	0.73	0.76	1.01	0.76	0.75	0.71	0.54	0.83	0.61	0.76	0.86	0.84	0.60
Dy	3.44	3.22	5.00	4.38	4.46	5.87	5.13	4.84	4.74	4.10	4.79	3.78	4.12	5.30	5.22	3.70
Ho	0.64	0.76	0.86	0.86	0.81	0.98	0.97	1.00	0.81	0.80	1.02	0.74	0.76	1.06	0.96	0.79
Er	1.98	2.01	2.44	2.42	2.23	2.36	2.80	2.50	2.31	2.06	2.59	2.00	2.13	2.90	2.82	2.49
Tm	0.21	0.23	0.27	0.30	0.27	0.29	0.35	0.30	0.33	0.27	0.35	0.28	0.31	0.39	0.36	0.38
Yb	1.62	1.79	1.89	2.06	1.76	1.73	2.58	2.28	2.04	1.97	2.37	1.83	1.86	2.70	2.47	2.56
Lu	0.22	0.25	0.25	0.27	0.22	0.28	0.32	0.25	0.35	0.21	0.34	0.25	0.26	0.37	0.37	0.37
$(La/Yb)_N$	4.30	2.60	8.62	7.32	11.56	19.18	6.42	5.93	8.74	5.21	6.90	5.61	5.81	6.23	6.84	
$(La/Sm)_N$	2.16	1.67	2.97	3.19	3.01	4.18	2.97	2.57	3.69	2.52	2.93	2.66	2.72	2.90	2.81	
$(Tb/Yb)_N$	1.37	1.19	1.76	1.52	1.85	2.50	1.26	1.41	1.49	1.17	1.50	1.43	1.75	1.36	1.45	
Eu/Eu*	1.31	1.15	1.19	1.23	1.09	1.25	1.19	1.17	1.31	1.21	1.21	1.35	1.32	1.22	1.12	

*International rock standard.

4.b. Rock nomenclature

The total alkali v. silica diagram recommended by the International Union of Geological Sciences (IUGS) for the classification of volcanic rocks (Le Bas *et al*. 1986) is adopted in this study. The basalt samples are restricted in composition and mostly fall in the alkali basalt field (Fig. 5a) according to the subdivision of Irvine & Baragar (1971). Compared with Cenozoic basalts from western Saudi Arabia (Camp, Roobol & Hooper, 1991), the Shalatein basalts closely match alkali olivine basalt from Harrat Kura and differ from the Harrat Ithanyn-Khaybar olivine transitional basalts, which have both alkaline and subalkaline varieties. A Zr/TiO_2 v. Nb/Y diagram (Winchester & Floyd, 1977) clearly indicates that the Shalatein basalts have an alkaline affinity (Fig. 5b).

4.c. Major and trace element variations

The Shalatein basalt samples have moderately high MgO (9.8–5 wt%), corresponding to Mg no. ranging from 65 to 46 (Table 1). They are characterized by high $Na_2O + K_2O$ contents (5.6–3.4 wt%) and Na_2O/K_2O (2.6–5.4; Table 1) and are thus sodic in nature. Estimated CIPW normative compositions (assuming an Fe^{+2}/Fe_{total} ratio of 0.75) are variable. Six samples contain normative hypersthene (0.1–8.3%) and olivine (17–4%), while the rest of the samples contain normative nepheline (1–12%). The least evolved rocks have higher degrees of silica undersaturation. The basalts show wide variations in TiO_2 (1.7–3.3 wt%), Al_2O_3 (13–18 wt%), P_2O_5 (0.2–0.78 wt%) Cr (229–34 ppm), Ni (239–44 ppm), Sc (31–15 ppm), Nb (100–11 ppm), La (49–6 ppm) and Zr (237–78 ppm). Variation diagrams (Fig. 6), using Mg no. as an index of differentiation, show a general increase of SiO_2, Al_2O_3, Sr, Nb, Y and Yb with decreasing Mg no. Elements compatible in olivine and clinopyroxene, (e.g. Ni, Cr, Ca) decrease with decreasing Mg no. The variation in total iron (as Fe_2O_3), TiO_2, P_2O_5, La and Th (elements compatible with Fe–Ti oxides and apatite) show an increase in the contents of these elements with decreasing Mg no. up to a maximum Mg no. of about 56 after which there is a slight decrease in the contents of these elements.

Chondrite-normalized REE patterns (Fig. 7a) for the Shalatein basalts are LREE-enriched with considerable LREE/HREE fractionation $(La/Yb)_N = 19.2–2.6$. There is a general systematic increase in the $(La/Yb)_N$ ratios with increasing differentiation in samples with Mg no. > 56; the least evolved sample (SH-15) shows the flattest REE pattern ($(La/Yb)_N = 2.6$). In samples with Mg no. < 56, the ratios $(La/Yb)_N$ decrease with increasing differentiation (Fig. 7b), a feature that most probably reflects apatite fractionation. All the samples display slightly positive Eu anomalies ($Eu/Eu^* = 1.09–1.35$), a feature recognized in many alkali basalt suites around the world, such as the Bonia Centre in Afar Rift, Ethiopia (Barberi *et al*. 1975). There is very little variation in HREE abundances, and a limited range in $(Tb/Yb)_N$ from 1.2 to 2.5. However, the LREE have slightly fractionated patterns ($(La/Sm)_N = 1.7–4.2$) with a pronounced variation compared to the HREE (Fig. 7a).

5. Discussion

5.a. Characterization of the magma source region

Continental intraplate alkali basalts are commonly considered to be the products of direct partial melting of the upper mantle either during major lithospheric extension and consequent rapid convective upwelling of the asthenosphere (Perry *et al*. 1990; Kent, Storey & Saunders, 1992), or when a mantle plume impinges on the base of the continental lithosphere (Morgan, 1981; McKenzie & Bickle, 1988; Campbell & Griffiths, 1990) causing partial melting, melt segregation and

https://doi.org/10.1017/S0016756802006994 Published online by Cambridge University Press

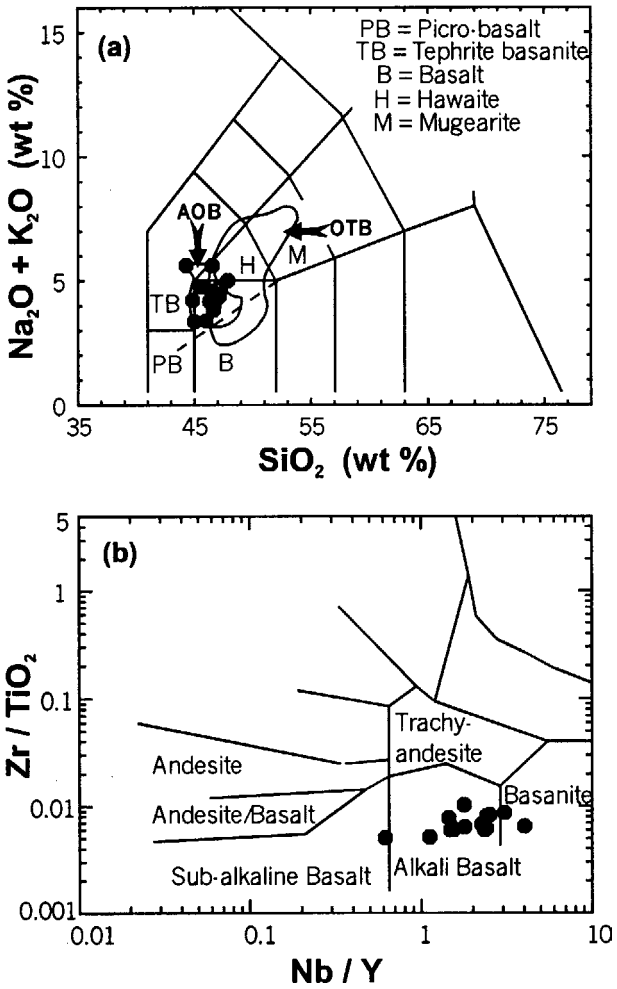

Figure 5. Chemical classification of the Shalatein basalts according to: (a) SiO_2 v. $Na_2O + K_2O$ (TAS) diagram of Le Bas *et al*. (1986); the dashed line in the basalt field is the alkaline/subalkaline field boundary of Irvine & Baragar (1971); the areas labelled alkali olivine basalts (AOB) and olivine transitional basalts (OTB) are for Saudi Arabian basalts from Harrat Kura and Harrat Khaybar-Ithanyan, respectively (Camp, Roobol & Hooper, 1991); (b) Zr/TiO_2 v. Nb/Y diagram (Winchester & Floyd, 1977).

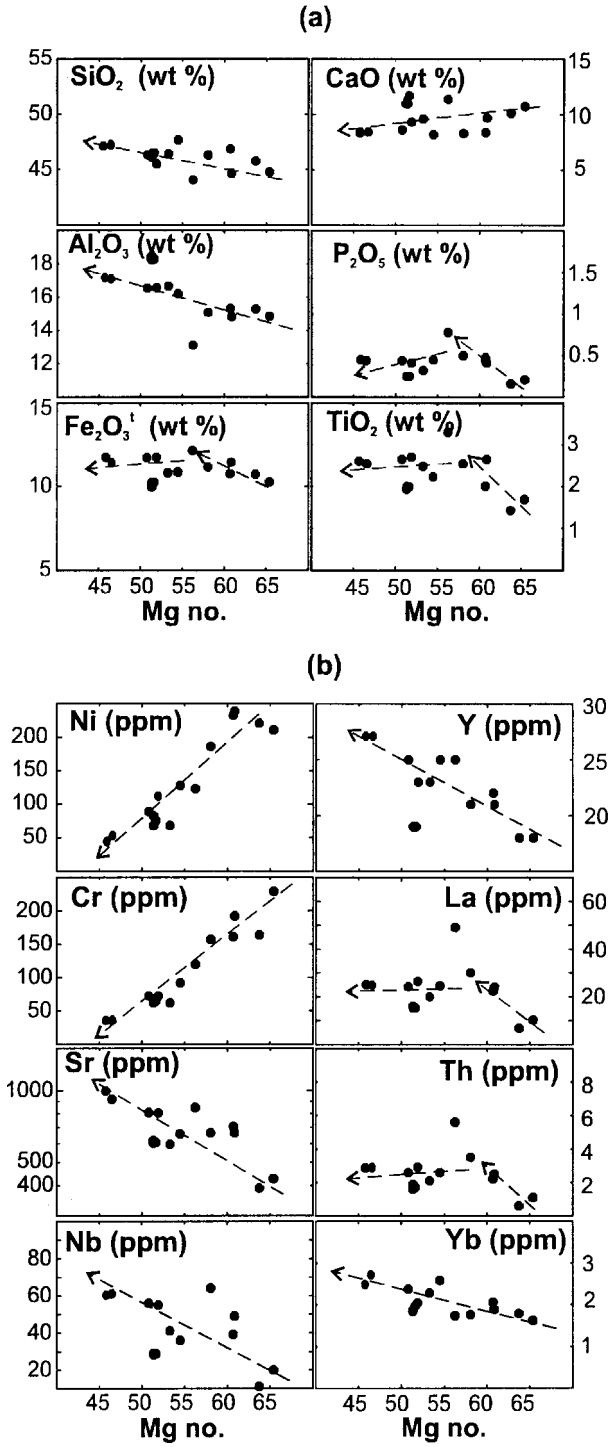

Figure 6. Mg no. (Mg no. = 100 Mg/(Mg + Fe^{2+}), assuming $Fe_2O_3/FeO = 0.2$) variation diagrams for: (a) selected major elements (wt%) and (b) trace elements (ppm) from the Shalatein basalts. The plotted trends are visual estimates.

possibly initiating rifting. Similarities between some OIB and continental basalts have led some authors to conceive a genetic link between the two; for example, Fitton & Dunlop (1985) envisage a common source for basalts from the oceanic and continental sectors of the Cameroon Line. Such a common source may be found in the well-mixed convective asthenosphere (Fitton, Dunlop & Leeman, 1991).

According to REE data (Table 2; Fig. 7) the source region of the Shalatein basalts should be located in the garnet–lherzolite zone (e.g. McKenzie & O'Nions, 1991). The range in $(Tb/Yb)_N$ of 1.2–2.5 is comparable with that of alkali basalts from Hawaii (Tb_N/Yb_N = 1.89–2.45: Frey *et al*. 1991), which are commonly considered to have been generated in a garnet-bearing lherzolitic mantle. This means a depth of at least 80 km (McKenzie & O'Nions, 1991), indicating that magma generation should have occurred well within the asthenosphere. Furthermore, studies based on geochemical and thermodynamic constraints (Arndt & Christensen, 1992; Anderson, 1994) have shown that extensive lithospheric participation in the melting process in continental areas is unlikely. Thus, it is

https://doi.org/10.1017/S0016756802006994 Published online by Cambridge University Press

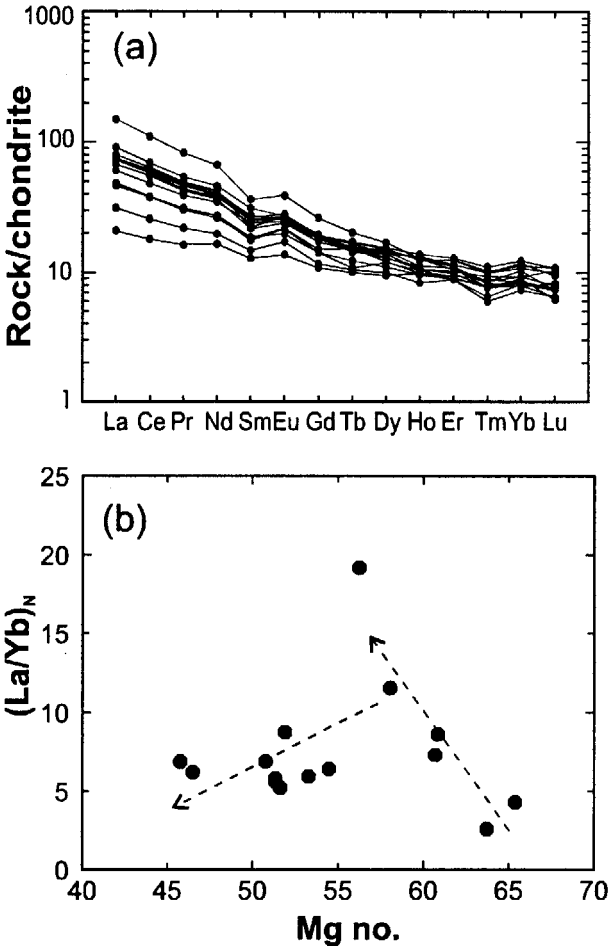

Figure 7. (a) Chondrite-normalized REE patterns for the Shalatein basalts. Normalization values are from Sun (1982); (b) Mg no. v. $(La/Yb)_N$ showing the evolution trends for mafic and evolved Shalatein basalts.

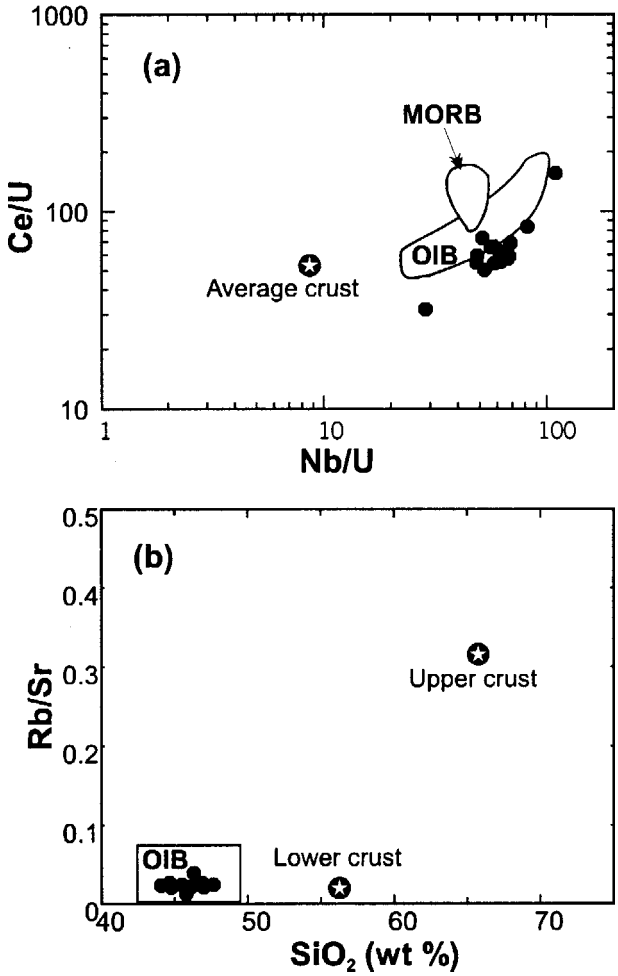

Figure 8. Binary diagrams of (a) Nb/U v. Ce/U for the Shalatein basalts, compared with MORB, average crust (Ito, White & Gobel, 1987; Hofmann *et al*. 1986) and OIB (Hofmann *et al*. 1986; Davies *et al*. 1989). (b) SiO_2 v. Rb/Sr for the Shalatein basalts compared with OIB (Fitton, Dunlop & Leeman, 1991) and upper and lower crust (Taylor & McLennan, 1985).

suggested that the source region of the basalt magmatism in the study area was the asthenosphere.

In order to explore the source characteristics of the Shalatein basalts based on their geochemical characteristics, critical trace element ratios are compared with those of well-known OIB occurrences (Fig. 8). Ce/U, Th/Nb and Rb/Sr are among the most useful ratios because they can be effective in distinguishing between mantle and crustal sources (Hofmann *et al*. 1986; McDonough, 1990). The Shalatein basalts have Ce/U ratios lower than N-MORB and mostly plot within the OIB field (Fig. 8a). They also show a restricted Rb/Sr ratio, which falls within the range of OIBs (Fig. 8b), providing an additional argument for their derivation from OIB-source mantle. They are distinctly different from the lower and upper crust.

The asthenospheric sources of OIB may be divided into four reservoirs on the basis of Sr, Nd and Pb isotopes. Two reflect enrichment by ancient crustal materials (EMI and EMII), one reflects addition of a subduction component with high $^{238}U/^{204}Pb$ (HIMU), and one is a depleted MORB mantle (DMM) (Hart, 1988). These types may also be identified using trace element ratios (Weaver, 1991). Comparison of the diagnostic element ratios with values for different types of OIB (Table 3) indicates that the Shalatein basalts may be derived from a HIMU source with slightly elevated Ba and K contents. Moreover, ratio–ratio plots of highly incompatible elements minimize the effects of inter-element fractionation during partial melting or fractional crystallization (Hole & LeMasurier, 1994). Figure 9 shows plots of Ba/Nb v. Ba/La and K/Nb for MORB, OIB end-members, and basalts from the study area. The diagrams reveal that the most important component in the source region of the Shalatein basalts is the one that has an HIMU-signature (Fig. 9a,b).

5.b. Origin of geochemical variations

The processes that may cause variations in the absolute and relative abundances of incompatible elements during the genesis of alkali basalts can be divided into three

https://doi.org/10.1017/S0016756802006994 Published online by Cambridge University Press

Table 3. Incompatible element ratios of the Shalatein basalts compared to ocean-island basalt end members

	Shalatein basalts		HIMU OIB		EMI OIB		EMII OIB			
	Range	Mean	Range	Mean	Range	Mean	Range	Mean	PM	N-MORB
Zr/Nb	7.1–2.3	4.2	5.0–3.2	4.1	11.4–4.2	6.9	7.3–4.5	6.1	14.8	30
La/Nb	0.68–0.41	0.51	0.66–0.77	0.72	1.19–0.64	0.94	1.09–0.89	0.98	0.94	1.07
Ba/Nb	8.5–5.0	5.7	6.5–4.9	5.6	17.7–5.6	13.2	11.0–7.3	9.7	9	4.3
Ba/Th	157–84	105	77–49	64	154–103	128	84–67	74	77	60
Rb/Nb	0.52–0.2	0.41	0.38–0.35	0.37	1.17–0.88	1.01	0.85–0.59	0.73	0.91	0.36
K/Nb	400–103	228	179–77	139	432–204	301	378–248	293	323	296
Th/Nb	0.07–0.05	0.05	0.101–0.078	0.09	0.122–0.105	0.112	0.157–0.111	0.134	0.117	0.071
Th/La	0.12–0.09	0.11	0.133–0.107	0.12	0.128–0.107	0.115	0.163–0.122	0.137	0.125	0.067
Ba/La	13.9–8.9	11.3	8.7–6.8	7.8	16.9–13.2	14.1	11.3–8.3	8.2	9.6	4

Values of OIB (HIMU, EMI, EMII), primordial mantle (PM), and mid-ocean ridge basalt (N-MORB) are from Weaver (1991).

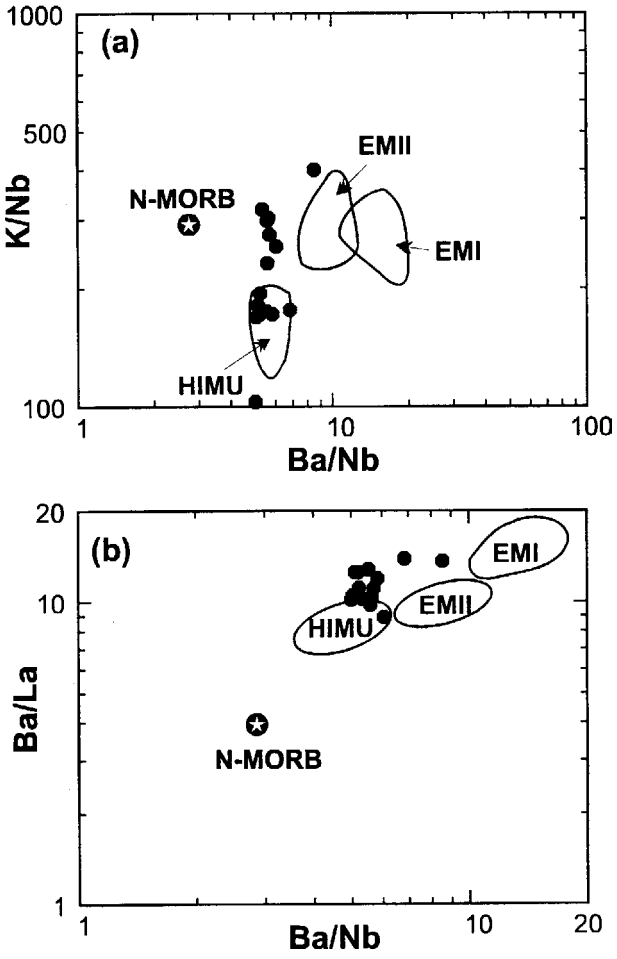

Figure 9. Binary diagrams of Ba/Nb v. (a) K/Nb and (b) Ba/La for the Shalatein basalts, compared with N-MORB and OIB end-members (HIMU, EMI and EMII). Data of N-MORB and OIB end-members are from Weaver (1991).

broad categories (Hole & LeMasurier, 1994). These are: (1) fractional crystallization; (2) different degrees of partial melting; and (3) interaction with the continental lithosphere.

5.b.1. Fractional crystallization

Petrographic evidence suggests that the evolution of the Shalatein basalts was predominantly a result of fractional crystallization. The basalts are generally porphyritic, and phenocryst assemblages show a gradual change from olivine to olivine–clinopyroxene-oxides and olivine–clinopyroxene–plagioclase. The geochemical data (Table 1; Fig. 6) illustrate the following features that are consistent with fractional crystallization: (1) the general trend of decreasing compatible trace elements (e.g. Cr and Ni) and increasing concentrations of incompatible elements (e.g. Nb, Y and Yb) with decreasing Mg no., suggesting olivine and/or clinopyroxene fractionation; (2) the transition from strongly incompatible to compatible behaviour of TiO_2 and P_2O_5, suggesting fractionation of Fe–Ti oxides and apatite; and (3) the transition from strongly incompatible to mildly compatible behaviour of La and Th probably caused by the compatible behaviour of LREE and Th during apatite crystallization (apatite has mineral-melt partition coefficients of 10–100 for REE: e.g. Fujimaki, 1986). Incompatible trace element data show that fractional crystallization becomes much more important at Mg no. $\approx$ 56 (Fig. 6). However, there is some variation in the more mafic samples that does not appear to be due primarily to fractional crystallization. Figure 10 displays a plot of Zr/Nb versus both Ce/Y and Nb/Y where strong negative trends with large variations in Ce/Y and Nb/Y are clear. Although clinopyroxene or amphibole removal may fractionate Ce/Y and Nb/Y ratios (Smedley, 1988), there is no petrographic evidence supporting amphibole fractionation in the basalts, and the range of Ce/Y and Nb/Y ratios requires unacceptably large amounts (> 90%, Fig. 10) of clinopyroxene fractionation. Therefore, fractional crystallization cannot be the only process producing the observed variations in the incompatible element ratios of the Shalatein basalts.

5.b.2. Different degrees of partial melting

Relative fractionation of HFSE is a common feature in both continental and oceanic basalts (e.g. Hawaii: Clague & Frey, 1982; Scotland: Smedley, 1988; Atlantic OIB: Weaver *et al*. 1987; North Sea: Latin, Dixon & Fitton, 1990; West Antarctica: Hole & LeMasurier, 1994). Such HFSE fractionation is considered to be a function of the amount of residual garnet

https://doi.org/10.1017/S0016756802006994 Published online by Cambridge University Press

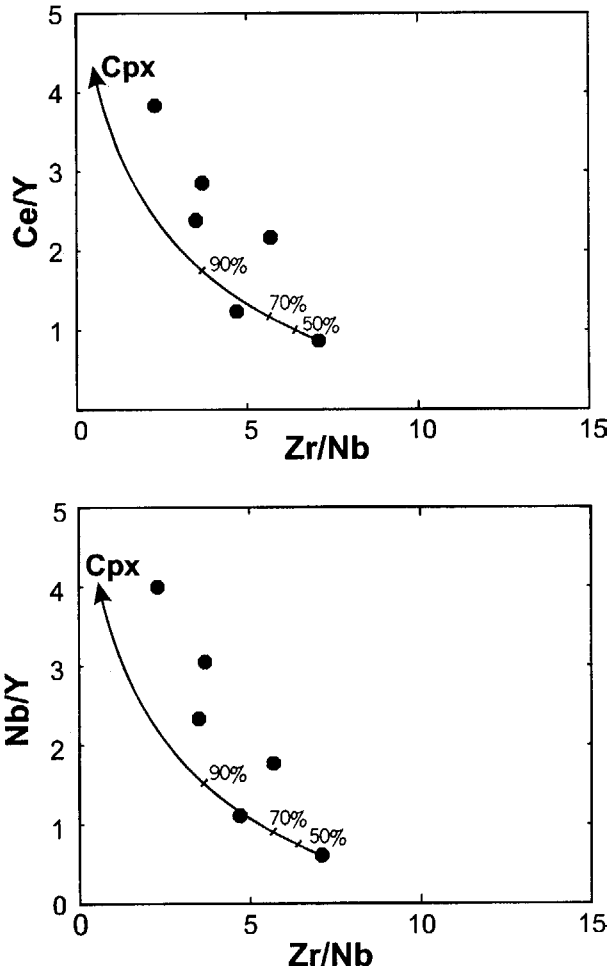

Figure 10. Binary diagrams of Zr/Nb v. (a) Ce/Y and (b) Nb/Y for mafic samples (Mg no. > 56). The vectors labelled Cpx represent fractional removal of clinopyroxene. The numbers along the trends indicate the fraction of clinopyroxene removed and are calculated using the simple Rayleigh crystal fractionation equation ($C_L/C_i = F(K_D-1)$) of Arth (1976), where C_L is the concentration of a trace element in the differentiated liquid, C_i is the initial concentration of trace element in the source, F is the fraction of liquid remaining and K_D is the bulk distribution coefficients of the fractionating minerals. The partition coefficients used are listed in Table 4.

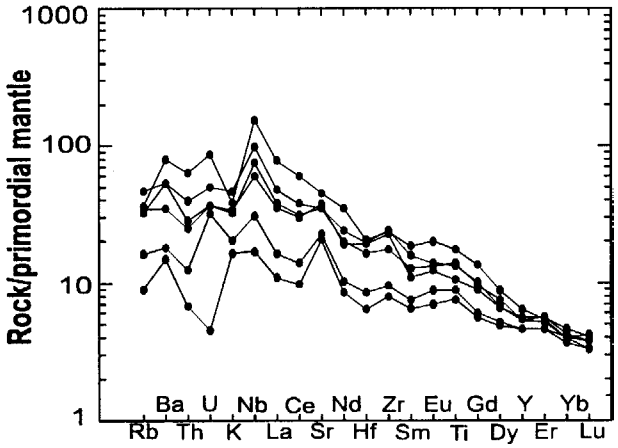

Figure 11. Primordial mantle-normalized patterns for mafic samples (Mg no. > 56) of the Shalatein basalts. Normalization values are from Sun & McDonough (1989).

and clinopyroxene in the mantle source as a result of different degrees of partial melting. Since Y is retained in garnet ($K_D = 1.083$: Frey, Green & Roy, 1978), the strong negative correlation (Fig. 10) between an index of partial melting such as Ce/Y and Nb/Y ratios (Cox & Hawkesworth, 1985; Smedley, 1988) and Zr/Nb in the Shalatein basalts suggests that the observed relative fractionation in such ratios is a function of degree of partial melting. Samples with the highest Ce/Y and Nb/Y and lowest Zr/Nb represent smaller degrees of partial melt whereas those having the lowest Ce/Y and Nb/Y and highest Zr/Nb represent larger degree melts.

Primordial mantle-normalized incompatible element profiles for the least fractionated samples (Fig. 11) show no evidence of lithospheric or subduction signatures, as they lack negative HFSE anomalies (Pearce, 1983). Most profiles display an overall similarity, being incompatible element-enriched with peaks at Nb and Sr, relative depletion in LILE (Rb, Ba, Th, U and K), and having little variation in Y contents. The narrow ranges in normalized HREE and Y concentrations suggest that garnet was present in the mantle source of the basalts. The profiles with the greatest incompatible element enrichments appear to have pronounced negative K anomalies. Such negative K anomalies are apparently a common feature of Si-undersaturated basic magmas (Fitton & Dunlop, 1985) and are frequently attributed to retention of K-bearing phases (e.g. phlogopite or K-rich amphibole) in the source reservoir during low degrees of partial melting. The fact that negative K anomalies occur in the more enriched profiles suggests that for smaller degrees of partial melting, such K-bearing phases may have been retained in the source, but with a greater degree of partial melting, they are consumed (Fitton & Dunlop, 1985; Smedley, 1988). In contrast, despite there being no petrographic evidence for plagioclase accumulation (a mineral with high K_DSr), most of the samples are characterized by strong positive Sr anomalies. Thus, the relatively high Sr content in these basalts is a feature inherited from the mantle source, and the high Sr content of the less enriched samples may be attributed to higher degrees of partial melting.

Modelling of some REE has been carried out (Fig. 12) in order to assess the effects of different degrees of partial melting of a garnet lherzolite source. The partial melting curves were constructed using the non-modal batch partial melting equation of Shaw (1970): $C_L/C_0 = 1/D_0 + F(1 - P)$, where C_L and C_0 are the concentration of a trace element in the melt and in the source, respectively; D_0 is the bulk distribution coefficient for the starting assemblage, F is the fraction of melting, and P is the bulk distribution coefficient of minerals that make up the melt. The modal mineralogy

https://doi.org/10.1017/S0016756802006994 Published online by Cambridge University Press

Table 4. Partition coefficients and REE (ppm) in the mantle source

	Ol	Opx	Cpx	Gt	PM
La	0.0004	0.002	0.054	0.01	0.55
Ce	0.0005	0.003	0.098	0.021	1.4
Nd	0.001	0.0068	0.21	0.087	1.08
Sm	0.0013	0.01	0.26	0.217	0.36
Eu	0.0016	0.013	0.31	0.32	0.13
Tb	0.0015	0.019	0.31	0.75	0.084
Yb	0.0015	0.049	0.28	4.03	0.372
Lu	0.0015	0.06	0.28	5.5	0.057
Zr			0.12		
Y			0.195		
Nb			0.01		

Primitive mantle (PM): McKenzie & O'Nions (1991); partition coefficient: Irving (1978), Hanson (1980), Frey, Green & Roy (1978).

of the mantle lherzolite source (59.5% olivine, 19.8% orthopyroxene, 13.5% clinopyroxene, 7.2% garnet) and the weight fraction of liquid contributed by each phase during melting (olivine = 0.78%, orthopyroxene = 5.22%, clinopyroxene = 47%, garnet = 47%) are taken from Kostoupoulos (1991) and Williamson *et al*. (1995). The abundances of REE in the source (PM) are listed, together with the partition coefficients, in Table 4. The primitive mantle values correspond to the Bulk Earth abundances of McKenzie & O'Nions (1991) and are roughly double the chondrite abundances (Kay & Gast, 1973). The data indicate a close match between the REE calculated at variable degrees of partial melting (F = 0.5–6%) and those in the Shalatein basalts. The lower Yb and Lu abundances in the calculated curves can be attributed to higher modal garnet in the model source relative to that of the Shalatein basalts.

It must be emphasized that the interpretation of Figure 12 is entirely model-dependent. The absolute position of the curves changes significantly according to the chosen values of C_0 and D. Thus no importance

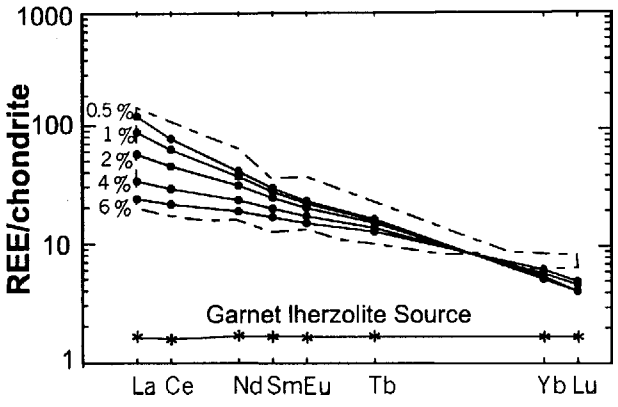

Figure 12. REE chondrite-normalized diagram illustrating different degrees of partial melting calculated by assuming non-modal batch melting of a garnet lherzolite source having REE contents of about two times chondrite (Williamson *et al*. 1995). The degree of melting (F) is indicated for each curve. The dashed line area is for mafic (Mg no. > 56) Shalatein basalts.

should be attached to the calculated F values in the diagram, or the absolute position of the curves. However, the diagram serves to illustrate that the wide variation in LREE can be attributed to different degrees of partial melting.

5.c. Relationship to Afro-Arabian rift system

It is important to relate magmatic/tectonic events in the Red Sea area to those of the Yemen, Ethiopia and Kenya areas (Afro-Arabian rift system). In these areas, volcanic activity began in the Late Eocene (44–38 Ma) and continued until 16 Ma (Mohr, 1983; Chiesa *et al*. 1989). The main episode of flood basalt volcanism took place in the period from 31 to 29 Ma (Baker, Snee & Menzies, 1996). Subsequent uplift occurred at less than 5 Ma, and a second phase of basaltic volcanism occurred at 4.5 Ma, associated with the modern phase of sea-floor spreading in the Red Sea (Mohr, 1983). In Saudi Arabia, extensive continental alkali basalts, known as Harrats (Camp & Roobol, 1991), were extruded during two distinct phases, the first from 30–20 Ma and the second from 12 Ma to Recent times. White & McKenzie (1989) suggested a comprehensive model for the volcanism, rifting and sea-floor spreading of the Red Sea–Gulf of Aden region in terms of a large mantle plume centered on the Afar triangle in Ethiopia. Despite the much greater volumes of magmatic rocks in Yemen, Arabia and Ethiopia compared to those along the Red Sea coast of Egypt, the similarity in age (Oligo-Miocene) may imply similar conditions in petrogenesis. Furthermore, studies based on the isotopic composition of basaltic rocks from the Afro-Arabian rift system, that is, the Ethiopian rift (Hart *et al*. 1989) and southern Yemen (Chazot & Bertrand, 1993), show that these basalts contain EMI and EMII components in their source. Vidal *et al*. (1991) and Schilling *et al*. (1992) suggested the presence of a HIMU-type mantle beneath the Afar region. Although the suggested HIMU source for the Shalatein basalts needs to be evaluated by radiogenic isotope studies, its presence beneath the study area indicates similarity to that beneath the Afar region and further supports the same history and source.

The instantaneous head diameter of mantle plumes is usually quoted as 1000–2000 km (Campbell & Griffiths, 1990; White & McKenzie, 1989). Thus, a model for the hot asthenosphere source in the origin of the Shalatein basalts in Egypt involves convective flow emanating from the Afar mantle plume in Ethiopian to produce an elongated and extended lobe of hot asthenosphere beneath northeastern Africa and Arabia (Camp & Roobol, 1992).

6. Conclusions

(1) The Shalatein alkali olivine basalts are porphyritic with phenocryst assemblages bearing

https://doi.org/10.1017/S0016756802006994 Published online by Cambridge University Press

evidence of the crystallization order: olivine–clinopyroxene–Fe-Ti-oxides–plagioclase.

(2) There is no evidence of significant crustal contamination or interaction with subcontinental lithosphere. The basalt compositions can be modelled by melting of an asthenospheric garnet lherzolite with HIMU affinities.

(3) Variations in the basalt composition arise from different degrees of partial melting, and fractional crystallization.

(4) The Shalatein basalts probably represent part of the Afro-Arabian rift system, which has been formed due to a large mantle plume centred beneath the Afar triangle in Ethiopia.

Acknowledgements. Fieldwork would not be possible without the help of the Egyptian Geological Survey and Mining Authority. I am grateful to Dr R. Rifai for his help during fieldwork. Thanks are also due to Prof. A. El Bouseily for numerous helpful discussions and Prof. A. Hashad for his help in doing the chemical analyses in Canada. Dr P. Hooper and Dr R. White are greatly acknowledged for their valuable and constructive reviews that greatly improved the manuscript.

References

ABDEL AAL, A. Y. 1988. Characteristics and age of the volcanic rocks of South El-Quseir, Red Sea coastal plain, Egypt. *Egyptian Journal of Geology* **32**, 27–48.

ABDEL MONEM, A. A. & HEIKAL, M. A. 1981. Major element composition, magma type and tectonic environment of the Mesozoic to Recent basalts, Egypt: a review. *Bulletin of the Faculty of Earth Sciences, King Abdelaziz University, Jeddah* **4**, 121–48.

ABU ZEID, K., EL SAYED, H., RAMADAN, M., ZAHRA, H., EL GAMMAL, A. & EL KONY, S. 2000. Geology of Ras Benas-Abraq area. *Geological Survey of Egypt, internal report* 62/2000, 124 pp.

ALMOND, D. C. 1986. Geological evolution of the Afro-Arabian dome. *Tectonophysics* **131**, 301–32.

ANDERSON, D. L. 1994. The sublithospheric mantle as the source of continental flood basalts; the case against the continental lithosphere and plume head reservoirs. *Earth and Planetary Science Letters* **123**, 269–80.

ARNDT, N. T. & CHRISTENSEN, U. 1992. The role of sublithospheric mantle in continental flood volcanism: thermal and geochemical constraints. *Journal of Geophysical Research* **97**, 10967–81.

ARTH, J. G. 1976. Behavior of trace elements during magmatic processes – a summary of theoretical models and their applications. *Journal of Research, United States Geological Survey* **4**, 41–7.

BAKER, J., SNEE, L. & MENZIES, M. 1996. A brief Oligocene period of flood volcanism in Yemen: Implications for the duration and rate of continental flood volcanism at the Afro-Arabian triple junction. *Earth and Planetary Science Letters* **138**, 39–55.

BALDRIDGE, W., EYAL, Y., BARTOV, Y., STEINITZ, G. & EYAL, M. 1991. Miocene magmatism of Sinai related to the opening of the Red Sea. *Tectonophysics* **197**, 181–201.

BARBERI, F., FERRARA, G., SANTACROCE, R., TREUIL, M. & VARET, J. 1975. A transitional basalt–pantellerite sequence of fractional crystallization, the Boina center, (Afar rift, Ethiopia). *Journal of Petrology* **16**, 22–56.

BOHANNON, R. G. 1986. Tectonic configuration of the western Arabian continental margin, southern Red Sea. *Tectonics* **5**, 477–99.

CAMP, V. E. & ROOBOL, M. J. 1991. Geologic map of the Cenozoic lava field of Harrat Rahat, Kingdom of Saudi Arabia. *Saudi Arabian Directorate General of Mineral Resources Geoscience Map* **GM-123**, scale 1:250,000, with text, 37 pp.

CAMP, V. E. & ROOBOL, M. J. 1992. Upwelling asthenosphere beneath Western Arabia and its regional implications. *Journal of Geophysical Research* **97**, 15255–71.

CAMP, V. E., ROOBOL, M. J. & HOOPER, P. R. 1991. The Arabian continental alkali basalt province: Part II. Evolution of Harrat Khaybar, Ithnayan, and Kura, Kingdom of Saudi Arabia. *Geological Society of America Bulletin* **103**, 363–91.

CAMPBELL, J. H. & GRIFFITHS, R. W. 1990. Implications of mantle plume structure for the evolution of flood basalts. *Earth and Planetary Science Letters* **99**, 79–93.

CHAZOT, G. & BERTRAND, H. 1993. Mantle sources and magma-continental crust interaction during early Red Sea–Gulf of Aden rifting in southern Yemen: elemental and Sr, Nd, Pb isotope evidence. *Journal of Geophysical Research* **98**, 1819–35.

CHIESA, S., CIVETTA, L., DE FINO, M., LA VOLPE, L. & ORSI, G. 1989. The Yemen trap series: genesis and evolution of a continental flood basalt province. *Journal of Volcanology and Geothermal Research* **36**, 337–50.

CLAGUE, D. A. & FREY, F. A. 1982. Petrology and trace element geochemistry of the Honolulu volcanics: implications for the oceanic mantle below Hawaii. *Journal of Petrology* **23**, 447–504.

COLEMAN, R. G., FLECK, R. J., HEDGE, C. E. & GHENT, E. D. 1977. The volcanic rocks of southwest Saudi Arabia and the opening of the Red sea. *Red Sea Research 1970–1975, Saudi Arabian Directorate General of Mineral Resources Bulletin* **22**, D1–D30.

COLEMAN, R. G., GREGORY, R. T. & BROWN, G. F. 1983. Cenozoic volcanic rocks of Saudi Arabia. *Saudi Arabian Deputy Ministry for Mineral Resources Open File Report* **03-93**, 82 pp.

COX, K. & HAWKESWORTH, C. J. 1985. Geochemical stratigraphy of the Deccan Traps at Mahabeleshwar, Victoria, Australia. *American Journal of Science* **275**, 461–9.

DAVIDSON, J. P., DUNGAN, M. A., FERGUSON, K. M. & COLUCCI, M. T. 1988. Crust-magma interactions and the evolution of arc magmas: The San Pedro–Pellado Volcanic complex, southern Chilean Andes. *Geology* **15**, 443–6.

DAVIDSON, J. P., FERGUSON, K. M., COLUCCI, M. T. & DUNGAN, M. A. 1987. The origin of magmas from the San Pedro–Pellado Volcanic complex, S. Chile: multicomponent sources and open system evolution. *Contributions to Mineralogy and Petrology* **100**, 429–45.

DAVIES, G. R., NORRY, M. J., GERALCH, D. C. & CLIFF, R. A. 1989. A combined chemical and Pb–Sr–Nd isotope study of the Azores and Cape Verde hotspots: the geodynamic implications. In *Magmatism in the ocean basins* (eds A. D. Saunders and M. J. Norry), pp. 231–56. Geological Society of London, Special Publication no. 42.

EL HINNAWY, E. & ABDEL MAKSOUD, M. A. 1972. Geochemistry of Egyptian Cenozoic basaltic rocks. *Chemie der Erde* **31**, 94–112.

FITTON, J. G. & DUNLOP, H. M. 1985. The Cameroon line, west Africa, and its bearing on the origin of oceanic and

continental alkali basalt. *Earth and Planetary Science Letters* **72**, 23–38.

FITTON, J. G., DUNLOP, H. M. & LEEMAN, W. P. 1991. Basic magmatism associated with Late Cenozoic extension in the western United States: compositional variations in space and time. *Journal of Geophysical Research* **96**, 13693–711.

FRANZ, G., PUCHELT, H. & PASTEELS, P. 1987. Petrology, geochemistry and age relations of Triassic and Tertiary volcanic rocks from SW Egypt and NW Sudan. *Journal of African Earth Sciences* **6**, 335–52.

FREY, F. A., GARCIA, M. O., WISE, W. S., KENNEDY, A., GURRIET, P. & ALBAREDE, F. 1991. The evolution of Mauna Kea volcano, Hawaii: petrogenesis of tholeiitic and alkali basalts. *Journal of Geophysical Research* **96**, 14347–75.

FREY, F. A., GREEN, D. H. & ROY, S. D. 1978. Integrated models of basalt petrogenesis: a study of quartz tholeiites to olivine melilitites from south-eastern Australia utilizing geochemical and experimental petrological data. *Journal of Petrology* **19**, 463–513.

FUJIMAKI, H. 1986. Partition coefficient of Hf, Zr, and REE between zircon, apatite and liquid. *Contributions to Mineralogy and Petrology* **94**, 42–5.

GHEBREAB, W. 1998. Tectonies of the Red Sea region reassessed. *Earth Science Reviews* **45**, 1–44.

GIERET, A. & LAMEYRE, V. 1985. Inverted alkaline–tholeiitic sequences related to lithospheric thickness in the evolution of continental rifts and oceanic islands. *Journal of African Earth Sciences* **3**, 261–8.

HAASE, K., MUHE, R. & STOFFERS, P. 2000. Magmatism during extension of the lithosphere: geochemical constraints from lavas of the Shaban Deep, northern Red Sea. *Chemical Geology* **166**, 225–39.

HAFEZ, A. M. & ABDOU, M. I. 1990. Geochemical characteristics of Oligocene and Cretaceous volcanics from Northern Egypt. *Annal of the Geological Survey of Egypt* **16**, 179–88.

HANAFY, M. A., YOUSEF, S. M. & GAD, A. M. 1996. Mineralogical and geochemical studies on the basaltic rocks of the Bahariya Oasis, Western Desert, Egypt. *Proceedings of the Geological Survey of Egypt Centennial Conference,* 331–50.

HANSON, G. N. 1980. Rare earth elements in petrogenetic studies of igneous systems. *Annual Review of Earth Science* **8**, 371–406.

HART, S. R. 1988. Heterogeneous mantle domains: signatures, genesis, and mixing chronologies. *Earth and Planetary Science Letters* **90**, 273–96.

HART, W. K., WOLDEGABRIEL, G., WALTER, R. C. & MERTZMAN, S. A. 1989. Basaltic volcanism in Ethiopia: constraints on continental rifting and mantle interactions. *Journal of Geophysical Research* **94**, 7731–48.

HOFMANN, A. W., JOCHUM, K. P., SEUFERT, M. & WHITE, W. M. 1986. Nb and Pb in oceanic basalts: new constraints on mantle evolution. *Earth and Planetary Science Letters* **79**, 33–45.

HOLE, M. J. & LEMASURIER, W. E. 1994. Tectonic controls on the geochemical composition of Cenozoic, mafic alkaline volcanic rocks from West Antractica. *Contributions to Mineralogy and Petrology* **117**, 187–202.

HUBBARD, H. B., WOOD, L. F. & ROGERS, J. J. W. 1987. Possible hydration anomaly in the upper mantle prior to Red Sea rifting: Evidence from petrologic modeling of the Wadi Natash alkaline basalt sequence of eastern Egypt. *Geological Society of America Bulletin* **98**, 92–8.

IRVINE, T. N. & BARAGAR, W. R. A. 1971. A guide to the chemical classification of the common volcanic rocks. *Canadian Journal of Earth Sciences* **8**, 523–48.

IRVING, A. J. 1978. A review of experimental studies of crystal/liquid trace element partitioning. *Geochimica et Cosmochimica Acta* **43**, 754–70.

ITO, E., WHITE, W. M. & GOBEL, C. 1987. The O, Sr, Nd and Pb isotope geochemistry of MORB. *Chemical Geology* **62**, 157–76.

KAY, R. W. & GAST, P. W. 1973. The rare earth element and origin of alkali basalts. *Journal of Geology* **81**, 653–82.

KENT, R. W., STOREY, M. & SAUNDERS, A. D. 1992. Large igneous provinces: sites of plume impact or plume incubation. *Geology* **20**, 891–4.

KOSTOPOULOS, D. K. 1991. Melting of the shallow upper mantle: a new prospective. *Journal of Petrology* **32**, 671–99.

LATIN, D. M., DIXON, J. E. & FITTON, J. G. 1990. Rift-related magmatism in the North Sea basin. In *Tectonic evolution of the North Sea rifts* (eds D. J. Blundell and A. D. Gibbs), pp. 102–44. Oxford, UK: Oxford Science Publications, Clarendon Press.

LE BAS, M. J., LE MAITRE, R. W., STRECKEISEN, A. & ZANETIN, B. 1986. A chemical classification of volcanic rocks based on the total alkalies–silica diagram. *Journal of Petrology* **27**, 745–50.

MACDOUGALL, J. D. 1988. Continental flood basalts and MORB: A brief discussion of similarities and differences in their petrogenesis. In *Continental Flood Basalts* (ed. J. D. MacDougall), pp. 331–41. Kluwer Academic Publishers.

MCDONOUGH, W. F. 1990. Constraints on the composition of the continental lithospheric mantle. *Earth and Planetary Science Letters* **101**, 1–18.

MCGUIRE, A. V. & STERN, R. J. 1993. Granulite xenoliths from western Saudi Arabia: the lower crust of the late Precambrian Arabian–Nubian Shield. *Contributions to Mineralogy and Petrology* **114**, 395–408.

MCKENZIE, D. & BICKLE, M. J. 1988. The volume and composition of melt generated by extension in the lithosphere. *Journal of Petrology* **29**, 625–79.

MCKENZIE, D. & O'NIONS, R. K. 1991. Partial melt distributions from inversion of rare earth element concentrations. *Journal of Petrology* **32**, 1021–91.

MENEISY, M. Y. 1990. Volcanicity. In *The Geology of Egypt* (ed. R. Said), pp. 157–72. Rotterdam: Balkema.

MENEISY, M. Y. & KREUZER, H. 1974. K–Ar ages of Egyptian basaltic rocks. *Geologisches Jahrbuch* **D9**, 21–31.

MOGHAZI, A. M., HASSANEN, M. A. & MOHAMED, F. H. 1997. Source and evolution history of some Mesozoic alkaline volcanics in the Eastern Desert of Egypt: inference from petrology and geochemistry. *Journal of African Earth Sciences* **24**, 11–28.

MOHAMED, F. H. 2001. The Natash alkaline volcanic field, Egypt: geochemical and mineralogical inferences on the evolution of a basalt to rhyolite eruptive suite. *Journal of Volcanology and Geothermal Research* **105**, 291–322.

MOHR, P. 1983. Ethiopian flood basalt province. *Nature* **303**, 577–84.

MORGAN, W. J. 1981. Hotspot tracks and the opening of the Atlantic and Indian Oceans. In *The oceanic lithosphere* (ed. C. Emiliani), pp. 443–87. New York: Wiley.

ORSZAG-SPERBER, F. & PLAZIAT, J.-C. 1990. La sédimentation continentale (Oligo-Miocene) des fossés du proto-rift du NW de la Mer Rouge. *Bulletin de la Société géologique de France* **8**, 385–96.

https://doi.org/10.1017/S0016756802006994 Published online by Cambridge University Press

OUDA, KH. & MASOUD, M. 1993. Sedimentation history and geological evolution of the Gulf of Suez during the late Oligo-Miocene. *Geological Society of Egypt, Special Publication* **1**, 47–88.

PALLISTER, J. 1987. Magmatic history of Red Sea rifting: Prospective from the central Saudi Arabian Coastal plain. *Geological Society America Bulletin* **98**, 400–17.

PEARCE, J. A. 1983. The role of subcontinental lithosphere in magma genesis at destructive plate margins. In *Continental basalt and mantle xenoliths* (eds C. J. Hawkesworth and H. J. Norry), pp. 230–49. Nantwich: Shiva.

PERRY, F. V., BALDRIDGE, W. S., DEPAOLO, D. J. & SHAFIQULLAH, M. 1990. Evolution of a magmatic system during continental extension: the Mount Taylor volcanic field, New Mexico. *Journal of Geophysical Research* **95**, 19327–48.

PURSER, B. H. & PHILOBBOS, E. 1993. The sedimentary expressions of rifting in the NW Red Sea. *Geological Society of Egypt, Special Publication* **1**, 1–45.

PURSER, B. H., PHILOBBOS, E. & SOLIMAN, M. 1990. Sedimentation and rifting in the NW parts of the Red Sea: a review. *Bulletin de la Société géologique de France* **8**, 371–84.

RESSETAR, R., NARIN, A. E. M. & MONARD, J. R. 1981. Two phases of Cretaceous–Tertiary magmatism in the Eastern Desert of Egypt: Paleomagnetic, chemical and K–Ar evidence. *Tectonophysics* **73**, 169–93.

SAID, R. 1962. *The Geology of Egypt.* Elsevier, 377 pp.

SAID, R. 1990. *The Geology of Egypt*. Rotterdam: Balkema, 734 pp.

SCHILLING, J. G., KINGSLEY, R. H., HANAN, B. B. & MCCULLY, B. L. 1992. Nd–Sr–Pb isotope variations along the Gulf of Aden: evidence for mantle–plume–continental lithosphere interaction. *Journal of Geophysical Research* **97**, 10927–66.

SHAW, D. M. 1970. Trace element fractionation during anatexis. *Geochimica et Cosmochimica Acta* **34**, 237–43.

SMEDLEY, P. L. 1988. Trace element and isotopic variations in Scottish and Irish Dinantian Volcanism: Evidence for an OIB-like mantle dource. *Journal of Petrology* **29**, 413–43.

SUN, S.-S. 1982. Chemical composition and origin of the Earth's primitive mantle. *Geochimica et Cosmochimica Acta* **46**, 179–92.

SUN, S.-S. & MCDONOUGH, W. F. 1989. Geochemical and isotopic systematics of oceanic basalts: implications for mantle composition and processes. In *Magmatism in the ocean basins* (eds A. D. Saunders and M. J. Norry), pp. 313–45. Geological Society of London, Special Publication no. 42.

TAYLOR, S. R. & MCLENNAN, S. M. 1985. *The continental crust: its composition and evolution.* Oxford: Blackwell, 312 pp.

VIDAL, P., DENIEL, C., VELLUTINI, P. J., PIGUET, P., COULON, C., VINCENT, J. & AUDIN, J. 1991. Changes of mantle sources in the source of rift evolution: the Afar case. *Geophysical Research Letters* **18**, 1913–16.

VOLKER, F., ALTHERR, R., JOCHUM, K.-P. & MCCULLOCH, M. T. 1997. Quaternary volcanic activity of the southern Red Sea: new data and assessment of models on magma sources and Afar plume-lithosphere interaction. *Tectonophysics* **278**, 15–29.

WEAVER, B. L. 1991. The origin of ocean island basalt end-member compositions: trace element and isotopic constraints. *Earth and Planetary Science Letters* **104**, 381–97.

WEAVER, B. L., WOOD, D. A., TARNEY, J. & JORON, J. L. 1987. Geochemistry of ocean island basalts from the South Atlantic: Ascension, Bouvet, St. Helena, Gough and Tristan da Cunha. In *Alkaline Igneous Rocks* (eds J. G. Fitton and B. G. J. Upton), pp. 253–67. Geological Society of London, Special Publication no. 30.

WHITE, R. & MCKENZIE, D. 1989. Magmatism at rift zones: The generation of volcanic continental margins and flood basalts. *Journal of Geophysical Research* **94**, 7685–729.

WILLIAMSON, M.-G., COURTNEY, R. C., KEEN, C. E. & DEHLER, S. A. 1995. The volume and rare earth concentrations of magma generated during finite stretching of the lithosphere. *Journal of Petrology* **36**, 1433–53.

WILSON, M. 1989. *Igneous petrogenesis.* London: Unwin Hyman, 457 pp.

WINCHESTER, J. A. & FLOYD, P. A. 1977. Geochemical discrimination of different magma series and their differentiation products using immobile elements. *Chemical Geology* **20**, 325–43.